ARTICLE
Journal of Cellular Biochemistry 106:232–246 (2009)

Journal of Cellular Biochemistry

PPARγ2 Nuclear Receptor Controls Multiple Regulatory Pathways of Osteoblast Differentiation From Marrow Mesenchymal Stem Cells

Keith R. Shockley,[1] Oxana P. Lazarenko,[2] Piotr J. Czernik,[3] Clifford J. Rosen,[1] Gary A. Churchill,[1] and Beata Lecka-Czernik[3]*

[1]*The Jackson Laboratory, 600 Main Street, Bar Harbor, Maine 04609*

[2]*Arkansas Children Hospital Research Institute, 1120 Marshall Street, Little Rock, Arkansas 72202*

[3]*Departments of Orthopaedic Surgery and Physiology and Pharmacology, Center for Diabetes and Endocrine Research, University of Toledo Medical Center, 3000 Arlington Ave., Toledo, Ohio 43614*

ABSTRACT

Rosiglitazone (Rosi), a member of the thiazolidinedione class of drugs used to treat type 2 diabetes, activates the adipocyte-specific transcription factor peroxisome proliferator-activated receptor gamma (PPARγ). This activation causes bone loss in animals and humans, at least in part due to suppression of osteoblast differentiation from marrow mesenchymal stem cells (MSC). In order to identify mechanisms by which PPARγ2 suppresses osteoblastogenesis and promotes adipogenesis in MSC, we have analyzed the PPARγ2 transcriptome in response to Rosi. A total of 4,252 transcriptional changes resulted when Rosi (1 μM) was applied to the U-33 marrow stromal cell line stably transfected with PPARγ2 (U-33/γ2) as compared to non-induced U-33/γ2 cells. Differences between U-33/γ2 and U-33 cells stably transfected with empty vector (U-33/c) comprised 7,928 transcriptional changes, independent of Rosi. Cell type-, time- and treatment-specific gene clustering uncovered distinct patterns of PPARγ2 transcriptional control of MSC lineage commitment. The earliest changes accompanying Rosi activation of PPARγ2 included effects on Wnt, TGFβ/BMP and G-protein signaling activities, as well as sustained induction of adipocyte-specific gene expression and lipid metabolism. While suppression of osteoblast phenotype is initiated by a diminished expression of osteoblast-specific signaling pathways, induction of the adipocyte phenotype is initiated by adipocyte-specific transcriptional regulators. This indicates that distinct mechanisms govern the repression of osteogenesis and the stimulation of adipogenesis. The co-expression patterns found here indicate that PPARγ2 has a dominant role in controlling osteoblast differentiation and suggests numerous gene-gene interactions that could lead to the identification of a ''master'' regulatory scheme directing this process. J. Cell. Biochem. 106: 232–246, 2009.

KEY WORDS: PPAR GAMMA; THIAZOLIDINEDIONES; OSTEOBLAST; BONE MARROW MESENCHYMAL STEM CELLS; GENE EXPRESSION

Peroxisome proliferator-activated receptor gamma (PPARγ) is a member of the nuclear receptor family of transcription factors, a large and diverse group of proteins that mediate ligand-dependent transcriptional activation and repression. PPARγ plays an important role in the control of adipocyte development as well as glucose and fatty acid metabolism [Rosen and Spiegelman, 2001]. Alterations in these pathways can lead to the development of obesity, insulin resistance, and Type 2 diabetes mellitus (T2D) [Sharma and Staels, 2007]. Activation of the PPARγ protein is essential for vital processes and affects cell proliferation, differentiation and neoplastic transformation [Lehrke and Lazar, 2005]. The discovery of significant cross-talk between PPARγ and other nuclear receptors, such as retinoid, estrogen, and the vitamin D receptors, strongly supports a pleiotropic role for this protein in the control of cell homeostasis [Gimble et al., 2006].

Additional Supporting Information may be found in the online version of this article.

Grant sponsor: NIH/NIA/NIAMS; Grant numbers: AG17482, AG028935; Grant sponsor: American Diabetes Association; Grant number: 1-03-RA-46; Grant sponsor: NIH/NHGRI Ruth L. Kirchstein Postdoctoral Fellowship; Grant number: HG003968.

*Correspondence to: Beata Lecka-Czernik, PhD, Department of Orthopaedic Surgery, University of Toledo Medical Center, Mail Stop 1095, 3000 Arlington Ave., Toledo, OH 43614. E-mail: Beata.LeckaCzernik@utoledo.edu

Received 23 June 2008; Accepted 15 October 2008 • DOI 10.1002/jcb.21994 • 2008 Wiley-Liss, Inc.

Published online 29 December 2008 in Wiley InterScience (www.interscience.wiley.com).

An essential role of PPARγ in the maintenance of bone homeostasis is implicated in animals and humans. In animal models, a decreased PPARγ activity leads to increased bone mass and osteoblast number [Akune et al., 2004; Cock et al., 2004], whereas increase in PPARγ activity due to treatment with the anti-diabetic thiazolidinedione (TZD) drug rosiglitazone (Rosi) results in significant decreases in BMD, bone volume and changes in bone microarchitecture [Rzonca et al., 2004; Soroceanu et al., 2004; Sottile et al., 2004; Ali et al., 2005]. This bone loss is associated with a decreased number of osteoblasts and an increased number of adipocytes [Rzonca et al., 2004; Ali et al., 2005].

In humans, an administration of TZDs results in progressive bone loss and diminished levels of circulating bone formation markers in older women [Schwartz et al., 2006; Grey et al., 2007]. The results of ADOPT studies, which evaluated the effectiveness of known anti-diabetic drugs on the maintenance of blood glucose levels in prediabetic patients, suggested that Rosi increased the frequency of fractures in women [Kahn et al., 2006, 2008]. Clinical studies of PPARγ gene polymorphisms in different human populations indicate a role for this transcription factor in the regulation of bone mass and predisposition to the bone loss in a high fat diet conditions [Rhee et al., 2005; Ackert-Bicknell et al., 2008].

The mechanism of TZDs-induced bone loss involves their effects on differentiation of bone cells. In cells of mesenchymal lineage, the TZD-activated PPARγ2 isoform induces adipocyte and suppresses osteoblast differentiation [Lecka-Czernik et al., 1999, 2002]. In cells of hematopoietic lineage, the TZD-activated PPARγ1 isoform positively regulates differentiation of osteoclasts [Wan et al., 2007]. Here, we analyzed the mechanistic consequences of Rosi activation of PPARγ2 on the global transcriptional response in a cellular model of marrow mesenchymal stem cell (MSC) differentiation. Using an ANOVA-based approach we describe time-dependent relationships in MSC-based gene expression and key aspects of cell conversion from osteoblast progenitor cells to mature adipocytes, including connections between genes and gene ontology groupings.

Our cellular model of PPARγ2 control of marrow MSC differentiation was originally developed to study the mechanisms by which PPARγ2 suppresses osteogenesis and promotes adipogenesis. However, we found that activation of this nuclear receptor by the exogenous ligand Rosi modulated gene expression for multiple pathways essential for regulation of cell homeostasis. Moreover, our results suggest that PPARγ2 has a profound effect on gene expression, even in the absence of exogenous ligand. These effects suggest a role in the modulation of MSC phenotype in conditions of increased PPARγ2 expression, including aging.

MATERIALS AND METHODS

CELL CULTURE, TREATMENT REGIME, AND RNA ISOLATION

Murine marrow-derived U-33 cells (previously referred as UAMS-33) represent a clonal cell line spontaneously immortalized in long term bone marrow cultures [Lecka-Czernik et al., 1999]. To study the effect of PPARγ2 on marrow mesenchymal stem cell differentiation, U-33 cells were stably transfected with either a PPARγ2 expression construct (U-33/γ2 cells) or an empty vector control (U-33/c cells), as described previously [Lecka-Czernik et al., 1999]. Several independent clones were retrieved after transfection and carefully analyzed for their phenotype. Clone 28.6 (representing U-33/γ2 cells) and clone γc2 (representing U-33/c cells) were used here. Experimental design, cell maintenance, cell treatment, and harvesting of RNA samples were described previously [Lecka-Czernik et al., 2007]. Primary bone marrow cultures were established from the bone marrow isolated from femora of 6 months old C57BL/6 mice, which were obtained from the colony maintained by the NIA under contractual agreement with Harlan Sprague Dawley, Inc. (Indianapolis, IN). Cultures of adherent bone marrow cells were maintained as previously described [Lazarenko et al., 2007]. After 10 days of growth, cells were treated with Rosi (1 μM) or vehicle (DMSO) for 3 days followed by RNA isolation [Lazarenko et al., 2007].

DNA MICROARRAY EXPERIMENTS

Microarray experiments were performed as described previously [Lecka-Czernik et al., 2007]. Briefly, RNA quality was assessed using the Agilent Model 2100 Bioanalyzer (Agilent Technologies, Palo Alto, CA). For each microarray 5 μg of total RNA was processed using the Affymetrix GeneChip® one-cycle target labeling kit (Affymetrix, Inc., Santa Clara, CA) according to the protocol recommended by the manufacturer. The resulting biotinylated cRNA was fragmented and hybridized to the GeneChip® Mouse Genome 430 2.0 Array (Affymetrix, Inc.). The arrays were washed, stained, and scanned using the Affymetrix Model 450 Fluidics Station and Affymetrix Model 3000 scanner by the University of Iowa DNA Core Facility according to the protocols recommended by the manufacturer. Probe intensity data were generated using the microarray suite (MAS) v5.0 software (Affymetrix, Inc.). The data is deposited in NCBI Gene Expression Omnibus (GEO) with accession number GSE10192.

TRANSCRIPT ABUNDANCE DIFFERENCES

The $2 \times 2 \times 3$ factorial design included the treatment (+/− Rosi), cell type (+/− PPARγ2) and time (2, 24, and 72 h) dimensions (see Fig. 1). Probe intensity data from all 24 Affymetrix GeneChip® arrays was read into the R software environment [Ihaka and Gentleman, 1996] directly from .CEL files using the R/affy package [Gautier et al., 2004]. Raw data quality was assessed using image reconstruction, histograms of raw signal intensities and MvA plots. Normalization was carried out using the robust multi-array average (RMA) method using all probe intensity data sets together [Irizarry et al., 2003] to form one expression measure per gene per array. Briefly, the RMA method was used to adjust the background of perfect match (PM) probes, apply a quantile normalization of the corrected PM values and calculate final expression measures using the Tukey median polish algorithm.

Log-transformed expression measures were expressed in fixed effects ANOVA models as the sum of different components contributing to the overall intensity value of each gene on the array [Kerr et al., 2000; Churchill, 2004]. First, the model:

$$Y_i = \mu + \text{CONDITION} + \varepsilon_i \quad (1)$$

was fit to the log-transformed gene expression measures Y_i across each of the 12 treatment conditions, where μ is the mean for each

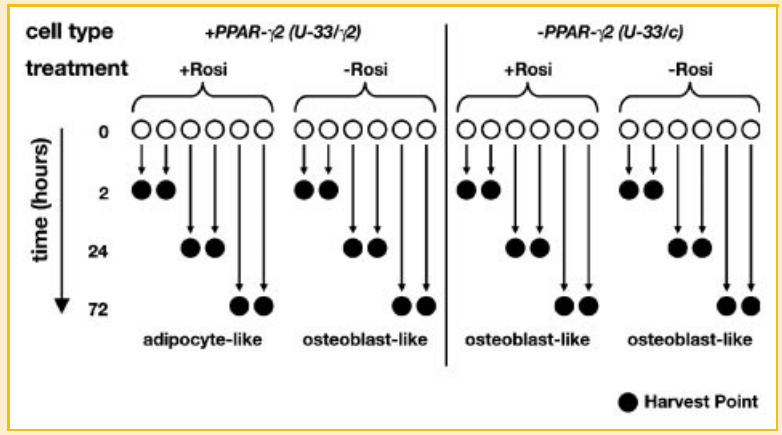

Fig. 1. Factorial design for the study of PPARγ2-induced cell differentiation in mesenchymal stem cell cultures. Marrow stromal cells transfected with PPARγ2 (U-33/γ2) or a control vector (U-33/c) were subjected to rosiglitazone (Rosi) to produce four different cell states. Replicate experiments were performed 2, 24, and 72 h after induction with Rosi to generate a total of 24 samples. Initial cell plating is showed as open circles and harvest points are shown as black circles.

array, CONDITION is the effect for treatment condition (e.g., +Rosi in U33/γ2 cells at 72 h) and ε_i captures random error. A modified F statistic (F_s) that assesses differential expression between treatment conditions was used as a statistical filter to select one probe set for each mapped Entrez gene on the array [Cui et al., 2005].

Other models were used to test focused research hypotheses. In these cases, the data was subset into the arrays corresponding to the experimental state (i.e., a specific condition/time combination) to be tested. For each time point (2, 24, and 72 h) a model was fit:

$$Y_i = \mu + \text{STATE} + \varepsilon_i \quad (2)$$

where STATE refers to a combination of cell type (i.e., U-33/c or U-33/γ2) and activation status (i.e., with or without Rosi). All statistical tests were conducted with F_s, a modified F-statistic incorporating shrinkage variance components that allows variance estimates to include information from all the probe sets on the array [Cui et al., 2005]. Critical *P*-values were calculated by permuting model residuals 1,000 times and pooling F-statistics [Yang and Churchill, 2007]. False discovery rate (FDR) values were estimated for each test result by implementing the "q-value" method of Storey [2002]. A probe set was considered to be differentially expressed for false discovery rates <0.01, unless otherwise noted.

DETERMINING EXPRESSION PATTERNS

k-means clustering was used to identify groups of differentially expressed transcripts that respond in a concerted manner. The k-means approach minimizes variation within a cluster and maximizes variation between clusters. A gene was assigned to a cluster if it was 70% stable over 1,000 bootstrap samples [Kerr and Churchill, 2001]. The proportion of variance explained ($\eta^2 = \sigma^2_{\bar{y}}/\sigma^2_y$) was used to choose an appropriate number of clusters. Here, η represents the ratio of the between groups sum of squares to the total sum of squares, where η^2 reduces to the correlation of multiple correlation (R^2) for linear relationships. η^2 was plotted versus k (see Fig. S1) in order to locate a value of "k" in an "elbow" structure with ~90% variance explained. Heat maps of clustering results were visualized in TreeView [Saldanha, 2004].

GO TERM ANALYSES

Over-represented classifications of genes were determined from statistical outcomes by testing for association with "biological process" gene ontology terms [Ashburner et al., 2000]. Mappings between Affymetrix probe sets, Entrez gene identifiers and GO terms were based on mouse Build 36 retrieved from the R/mouse4302 package built on March 15, 2007 (www.bioconductor.org). One Entrez identifier per probe set was used in the analysis, based on the maximum F_s statistic calculated using Equation (1). Hypergeometric tests for over-representation of GO terms were performed using the R/GOstats package [Falcon and Gentleman, 2007]. Unless specifically noted in the text, all enrichment analyses were based on a hypergeometric $P < 0.01$ significance criterion for groupings enriched with at least 5 genes.

We used a novel algorithm to quantify the hierarchical status of biological processes in the GO tree that we call a "modified GO slim" analysis. Our approach assigns a root to the GO tree based on either the presence of a gene in a term that is a common ancestor of two selected "GO slim" terms or a child of two "GO slim" terms (see Fig. S2). Using this approach, we found that the majority of the differentially expressed transcripts in our study were linked to one of ten biological process GO terms: "GO:0007165: signal transduction", "GO:0007049: cell cycle", "GO: 0002376: immune system process," "GO:0006629: lipid metabolism," "GO:0001501: skeletal development," "GO:0006091: metabolic energy generation," "GO:0008152: metabolism | GO:0006629: lipid metabolism" [i.e., GO:0008152 without (or conditional on) GO:0006629], "GO:0016043: cell organization and biogenesis," "GO:0051301: cell division" and "GO:0008283: cell proliferation" (see Fig. S3, Table S1). To increase interpretability, we excluded the following "unknown" GO terms ("GO: 0050874," "GO: 0051242," "GO: 0050791," "GO: 0051244," "GO: 0007582," "GO: 0043119," "GO: 0051243," and "GO: 0050875") and nonspecific terms ("GO:0048522: positive regulation of cellular process," "GO: 0009605: response to external stimulus," "GO:0009719: response to internal stimulus," "GO:0048519: negative regulation of biological process") from consideration.

INGENUITY PATHWAY ANALYSIS

The most significant biological categories of genes pertaining to changes due to activation of PPARγ2 with Rosi (false discovery rate <0.01) were determined by testing for association with high-level functions available in an expert-curated database of biological networks (Ingenuity Pathways Analysis™). The Ingenuity Pathways Knowledge Base (www.ingenuity.com) consists of expert-curated information from over 400 journals with known biological relationships between genes and gene products. A right-tailed Fisher's exact test for 2×2 contingency tables was used to determine the significance of overrepresentation of pathway members.

VALIDATION OF MICROARRAY DATA BY QUANTITATIVE REAL-TIME PCR

To validate gene expression results obtained from the microarray chips, an analysis of the expression levels of several chosen gene markers was performed using quantitative real-time PCR. This analysis was carried out with the same RNA samples that were analyzed on microarrays, as well as samples from two additional independent experiments performed in U-33/γ2 and U-33/c cells. In addition, the expression of the same gene markers was analyzed in primary bone marrow cells treated with Rosi or vehicle, as described above. Quantitative real time PCR was performed as described previously [Lazarenko et al., 2007]. Table S2 lists pairs of primers used for real time PCR validation of gene expression, whereas Table S3 shows the result of gene expression analysis. The expression of analyzed transcripts closely followed the expression detected on the microarrays and never exhibited change in an opposite direction (vs. the microarray) or gave rise to a change detected on the microarray that was not confirmed by PCR.

SEARCH FOR PEROXISOME PROLIFERATOR RESPONSE ELEMENTS

A search for peroxisome proliferator response elements (PPREs) was carried out using the Target Explorer program [Sosinsky et al., 2003]. DNA sequences spanning 8.0 kb regions upstream of the transcription start sites of the selected genes were obtained from GenBank database (National Center for Biotechnology Information, Bethesda, MD). A set of 15 characterized PPRE sequences was used to create a mononucleotide position weight matrix [Zandbergen et al., 2005]. The following PPREs were used: acyl-CoA oxidase (TGACCTTTGTCCT and TGACCTTCTACCT), fatty acid binding protein 4 (TGAACTCTGATCC), apolipoprotein I (TGACCCCTGCCCC), apolipoprotein II (CAACCTTTACCCT), liver fatty acid binding protein (TGACCTATGGCCT), enoyl-CoA hydratase-3hydroxyacyl-CoA dehydrogenase (TGAACTATTACCT), HMG-CoA synthase (AGACCTTTGGCCC), lipoprotein lipase (TGCCCTTTCCCCC), cytochrome P450IVA6 (TCACTTTTGCCCT, TGGCCTTTGTCCT, and TGACCTTTGCCCA), acyl-CoA synthetase (TGACTGATGCCCT), malic enzyme (TCAACTTTGACCC), and G0/G1 switch gene 2 (TGACCTTTGCAAT). Briefly, the algorithm aligns input sequences, looks for conservation of bases at certain positions and translates the alignment into a matrix. A positive weight implies that the frequency of a nucleotide at a given position is higher than the a priori probability of this base at that position. Motifs with a score of 6.0 or higher were recorded. The threshold score was chosen arbitrarily to accommodate less specific PPREs. Random sequences were generated using FaBox random sequence generator [Villesen, 2007]. Each of these sequences was 8 kb long and had a 45% GC content, which was similar to the length and GC content of the regulatory regions of the analyzed genes.

RESULTS

DETERMINING CONTRAST SETS

A system of U-33/γ2 and U-33/c cells represents a cellular model of MSC differentiation under the control of PPARγ2 transcription factor [Lecka-Czernik et al., 1999]. In basal conditions, both types of cells retain the parental osteoblastic phenotype of U-33 cells. However, treatment with the PPARγ agonist Rosi commits U-33/γ2 cells, but not U-33/c cells, towards adipocytes and irreversibly suppresses their osteoblastic phenotype [Lecka-Czernik et al., 1999]. Hence, comparing the transcriptomes of U-33/γ2 and U-33/c cells in the presence or absence of Rosi allowed us to study the exclusive effects of PPARγ2 on marrow MSC lineage allocation.

Our purpose was to find time-dependent relationships in gene expression due to PPARγ2-induced changes in cell phenotype. We addressed three principal questions. First, we sought to characterize the sequence of events which led from osteoblastic cells to cells of adipocytic lineage by Rosi-activated PPARγ2. Next, based on our previous work suggesting that PPARγ2 suppresses osteoblastogenesis and induces adipogenesis by distinct mechanisms [Lecka-Czernik et al., 2002; Lazarenko et al., 2006], we sought to identify gene candidates mediating PPARγ2 anti-osteoblastic activity versus genes mediating pro-adipocytic activity of this transcription factor. Finally, we asked whether PPARγ2 possesses either ligand-independent or endogenous ligand-dependent activities that influence the expression signature of marrow MSC.

Here, U-33/γ2 and U-33/c cells were cultured in the presence or absence of Rosi and gene expression was monitored at three different time points (2, 24, and 72 h) after exposure to the agonist (Fig. 1). Each time point corresponds to a separate stage of Rosi-treated U-33/γ2 cell conversion from the osteoblast-like phenotype to the adipocyte-like phenotype and includes induction (2 h), intermediate alterations in phenotype progression (24 h), and a terminally differentiated adipocytic phenotype with completely suppressed osteoblastic characteristics (72 h).

To begin, we defined a gene universe from the 45,037 probe sets on the microarray by mapping the putative transcripts to a total of 20,831 unique Entrez gene identifiers (see Materials and Methods Section). Next, pairwise contrasts between cell states were conducted at each time point to form three distinct *contrast sets* (Fig. 2). The expression patterns in Set 1 (U-33/γ2 + Rosi vs. U-33/γ2) and Set 3 (U-33/γ2 vs. U-33/c) provide a basis for addressing our principal research questions, while Set 2 (U-33/c + Rosi vs. U-33/c) is used as a control comparison.

A total of 4,252 and 7,928 genes were found to be differentially expressed at one or more time points in Set 1 and Set 3, respectively. The time-specific overlaps within both contrast sets show an abundance of differentially expressed transcripts after 72 h. In Set 1, a total of 147 (51), 822 (1,071), and 1,634 (2,096) genes are up

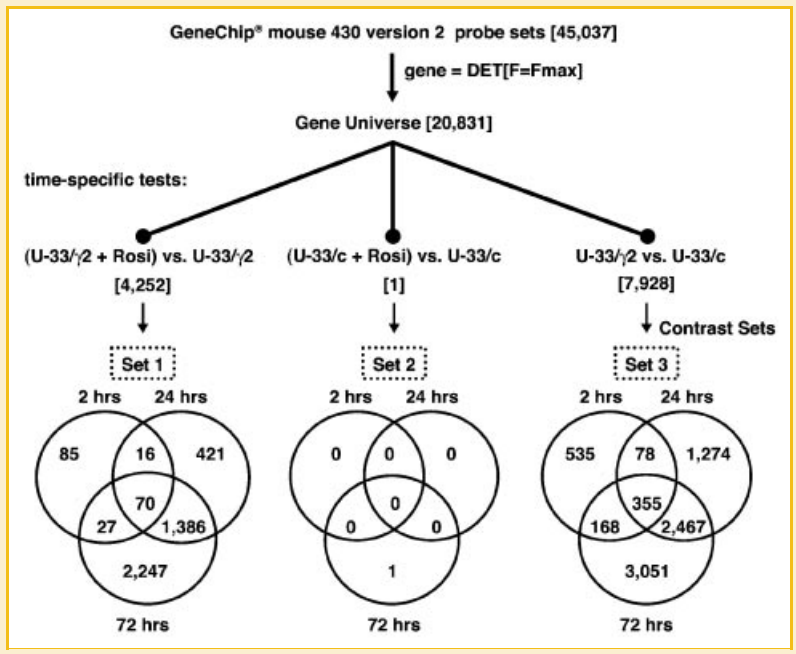

Fig. 2. Generation of contrast sets. A gene universe was selected based on mappings to Entrez gene identifiers (see Materials and Methods Section). When multiple differentially expressed transcripts (DETs) mapped to a single Entrez gene, the probe set with the largest F_s statistic across all conditions was chosen to represent the gene. Time-specific contrasts were used to find significant differences due to activation of the U-33/γ2 cell type [U-33/γ2 vs. (Rosi + U-33/γ2)] (Set 1), the presence of Rosi in U-33/c cells [U-33/c vs. (Rosi + U-33/c)] (Set 2), or between cell types [U-33/c vs. U-33/γ2] (Set 3). Overlapping and non-overlapping groups of time-specific differences between cell states are represented with Venn diagrams and referred to as *contrast sets*. Numbers in Venn diagrams refer to the number of differentially expressed transcripts.

(down-) regulated after 2, 24, and 72 h, respectively. In Set 3, a total of 626 (510), 1,907 (2,267), 2,686 (3,355) genes were up (down-) regulated after 2, 24, and 72 h, respectively. By contrast, only the expression of adiponectin (*adipoq.* + 38.7 at 72 h) was changed in Set 2. An increased expression of adiponectin, which is positively regulated by PPARγ [Sharma and Staels, 2007], in the absence of other transcriptional responses suggests either Rosi nonspecific effect or restricted activation of PPARγ1 isoform, which is naturally expressed in U-33/c cells. Nevertheless, the relative lack of differential expression in Set 2 supports our experimental methodology, since the ligand under investigation should not affect gene expression unless the studied transcription factor is present.

ACTIVATION OF U-33/γ2 CELLS WITH ROSI (CONTRAST SET 1)

Seven clusters explained ~88% of the variance in transcriptional patterns due to time-dependent treatment of U-33/γ2 cells with Rosi (Fig. 3A,B and Table S4). Genes in two clusters (Clusters 1 and 6) were increasingly upregulated over time with Rosi but not without Rosi. These clusters include genes associated with processes related to lipid and energy metabolism. Two clusters (Clusters 5 and 3) showed genes that were up- (or down-) regulated after 24 h and returned to their early expression level after 72 h treatment with Rosi while steadily increasing (or decreasing) without Rosi. Cluster 5 includes genes associated with immune processes, skeletal development, cell organization and biogenesis, and cell proliferation. Genes in Cluster 3 are associated with cellular biogenesis, lipid metabolism and energy generation. Finally, genes in the remaining three clusters were mostly downregulated over time with Rosi, but showed increasing (Cluster 7) or decreasing (Clusters 2 and 4) expression levels without Rosi. These genes are associated with metabolism and cell proliferation (Cluster 7), cell division, cell cycle and biogenesis (Cluster 2), and metabolism, skeletal development, and signal transduction (including TGFβ and G-protein signaling, and regulation of MAPK activity) (Cluster 4).

DIFFERENCES BETWEEN CELL TYPE (CONTRAST SET 3)

At the beginning of treatment, cells in both cultures exhibited 80% confluency and were exposed to fresh medium. Therefore, the pattern of genes differentially expressed at 2 h should reflect basic differences between the two cell lines during the late exponential phase of growth. Although both cell types experienced slower growth after 24 h, this intermediate time point reflects basal differences between cell lines and changes due to growth inhibition. However, after 72 h both types of cells were in the confluent stage, possessing a fibroblast-like morphology and a termination of cell division. Thus, in contrast to 2 and 24 h, the 72 h time point reflects phenotypic differences between cell lines, without the confounding effect of growth rate.

Seven clusters explain about 89% of the variance in differential transcription corresponding to Set 3 (Fig. 4A,B and Table S5). Clusters 4 and 7 contain genes with expression levels that are unchanged without PPARγ2 but increased dramatically with PPARγ2. Significant biological processes associated with these

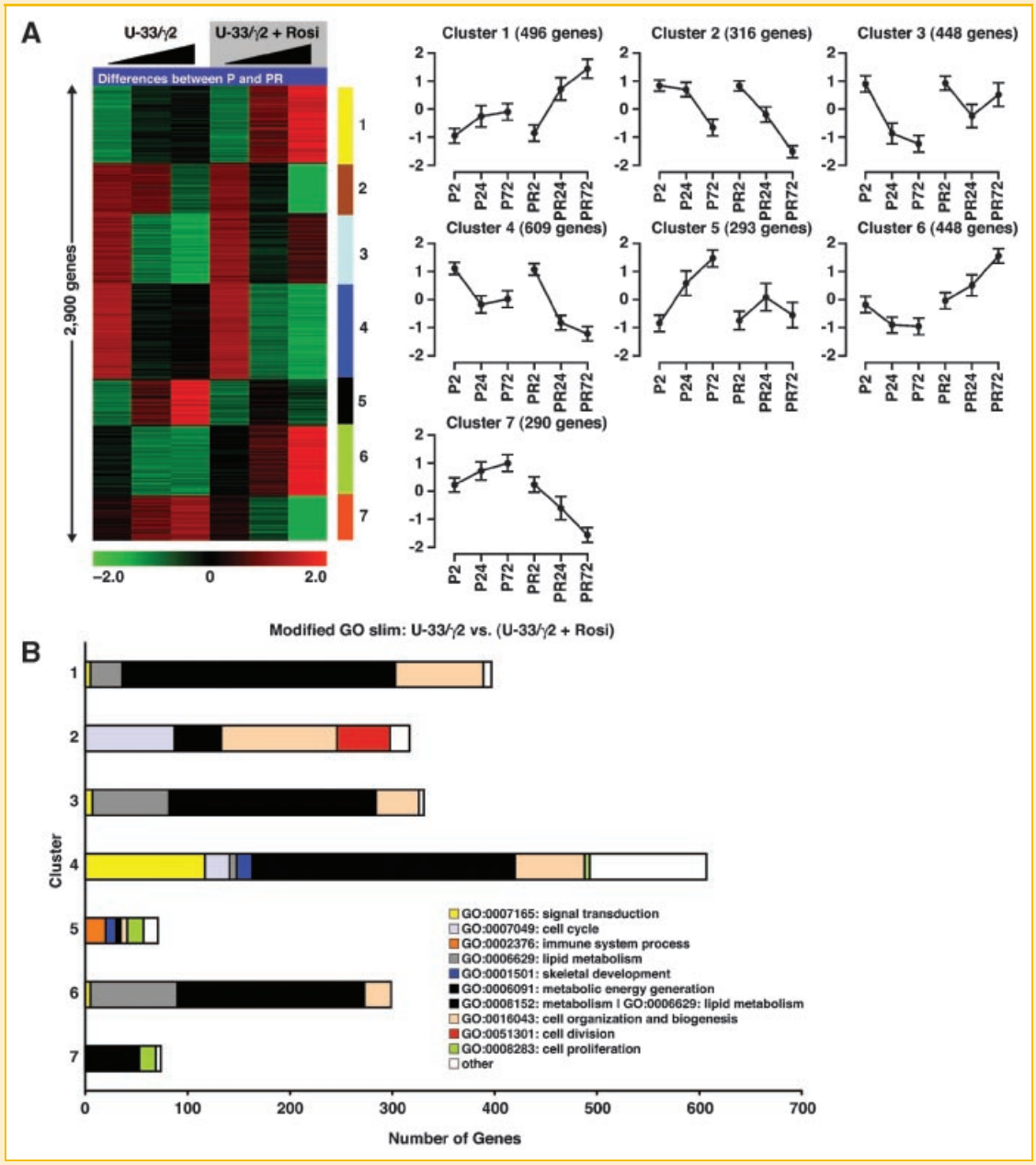

Fig. 3. Clustering of expression estimates due to activation of U-33/γ2 cells with Rosi. A: A heat map and k-means clustering of $\log_2$ transformed expression estimates standardized across conditions for activated U-33/γ2 versus inactivated U-33/γ2 cells at each harvest point. Time (2, 24, or 72 h) is indicated with a black triangular symbol above each heat plot. B: A modified GO slim analysis was used to describe prevailing biological processes in each cluster (see Materials and Methods Section). The percentage of genes from each cluster in (A) that can be interpreted with the modified GO slim procedure is shown next to each bar. In (B) the total number of genes shown for each cluster may exceed the number of genes in each cluster from (A) due to the many-to-one and one-to-many mapping relationships between genes and GO terms.

clusters include metabolism and inflammatory response (Cluster 4) and cell biogenesis and signal transduction including G-protein coupled receptor protein signaling (Cluster 7). Clusters 1, 3, 5, and 6 are characterized by significant decrease in gene expression in the presence of PPARγ2 and modest changes in gene expression in the absence of PPARγ2. Genes in these clusters are associated with lipid metabolism, biogenesis, cell cycle and intracellular signaling, including regulation of MAPK activity and apoptosis. Finally, genes in Cluster 2 show increasing expression with and without PPARγ2, but a higher increase over time without PPARγ2. These genes are involved in regulation of transcription regulation of metabolism and bone remodeling.

ROSI EFFECT ON DIFFERENTIAL EXPRESSION OF OVER-REPRESENTED GENE CATEGORIES IN U-33/γ2 CELLS

The Ingenuity Pathways Knowledge Base (IPKB) was used to classify over-represented genes into high-level functions reflecting functional relationships between genes and gene products (Table I).

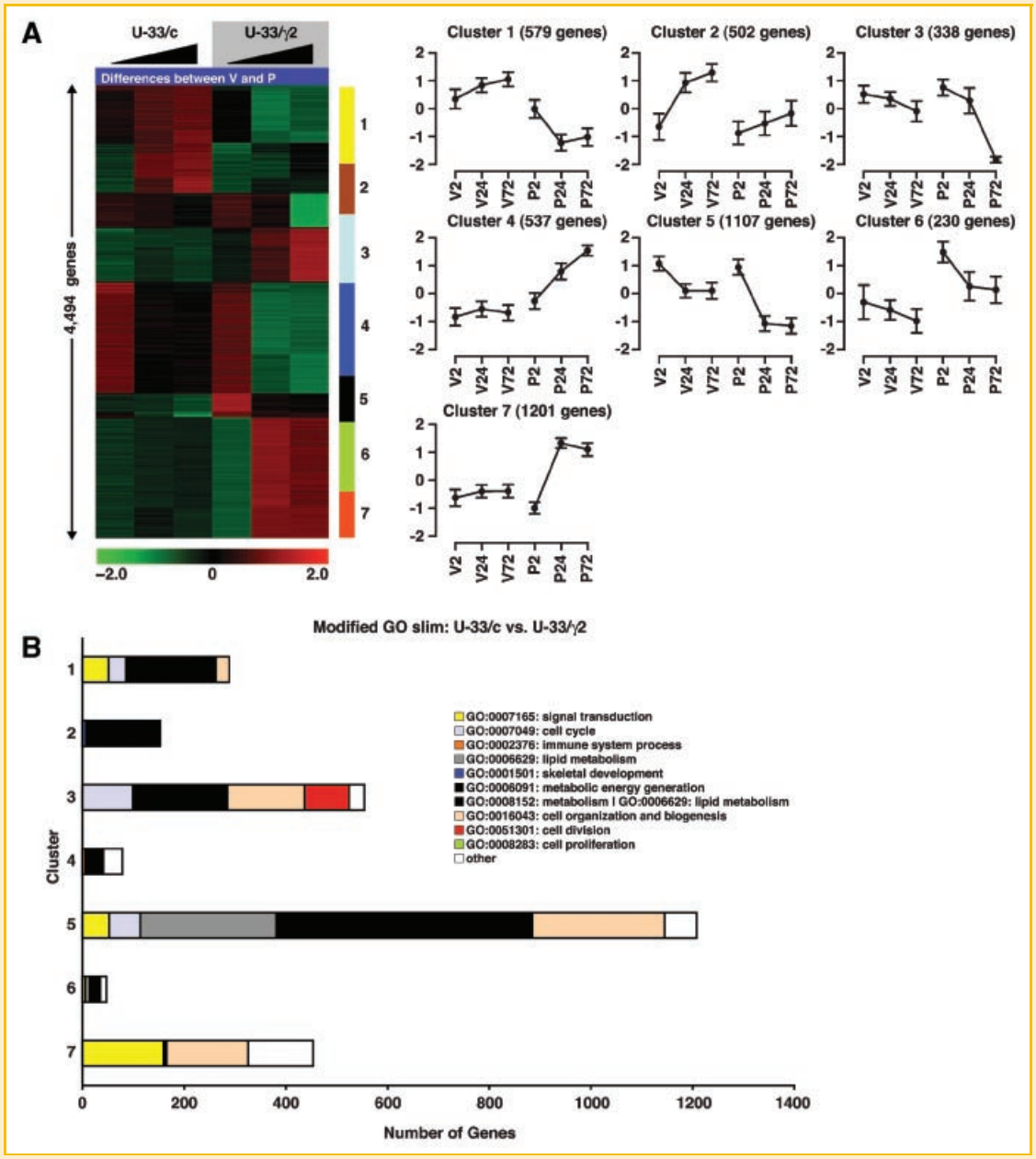

Fig. 4. Clustering of expression estimates due to differences between cell types. A: Heat map and k-means clustering of $\log_2$ transformed expression estimates standardized across conditions for un-induced U-33/γ2 versus U-33/c cells at each harvest point. Time (2, 24, or 72 h) is indicated with a black triangular symbol above each heat plot. B: A modified GO slim analysis was used to describe prevailing biological processes in each cluster (see Materials and Methods Section). The percentage of genes from each cluster in (A) that can be interpreted with the modified GO slim procedure is shown next to each bar.

Genes found in Lipid Metabolism and Carbohydrate Metabolism categories are induced early and are consistently upregulated, reflecting PPARγ2 proadipocytic activity and its role in the control of energy metabolism. The expression of genes in the Skeletal and Muscular System Development and Function category is affected in a manner that is consistent with the known function of these genes and anti-osteoblastic activity of PPARγ2. Positive regulators of osteoblast development are downregulated (e.g., Wisp1, Dmp1, and BMP4), whereas genes with a known or potential role in the negative regulation of this process are upregulated (e.g., Tob1 and Tle3) (see Table IV). In addition, Rosi affects the expression of a significant number of genes controlling cell growth and proliferation; both processes are required for osteoblast differentiation. Interestingly, besides gene categories closely related to fat and bone cell differentiation, PPARγ2 also regulates the expression of a large number of genes controlling cell death and cancer, as well as connective tissue, immune, nervous and cardiovascular systems development.

TABLE I. Ingenuity High Level Functional Categories: (U-33/γ2 + Rosi) Versus U-33/γ2

Category	Number of members (up/down)		
	2 h	24 h	72 h
Lipid metabolism	23 (23/-)	99 (99/-)	156 (156/-)
Carbohydrate metabolism	13 (13/-)	59 (59/-)	82 (82/-)
Skeletal and muscular system development and function	19 (7/12)	111 (24/87)	205 (22/183)
Differentiation of osteoblast	2 (2/-)	9 (9/-)	29 (10/19)
Development of skeleton	6 (-/6)	39 (-/39)	71 (-/71)
Ossification	3 (-/3)	23 (-/23)	38 (-/38)
Mineralization of bone	—	—	15 (-/15)
Cellular growth and proliferation	50 (29/21)	356 (56/300)	549 (24/525)
Cell death	54 (31/23)	366 (122/247)	493 (28/465)
Connective tissue development and function	27 (18/9)	139 (54/85)	263 (66/197)
Immune and lymphatic system development	25 (15/10)	15 (9/6)	122 (2/120)
Immune response	23 (11/12)	55 (-/55)	123 (2/121)
Cancer	55 (32/23)	529 (125/404)	694 (39/655)
Nervous system development and function	6 (2/4)	49 (-/49)	72 (-/72)
Cardiovascular system development and function	11 (4/7)	84 (15/69)	151 (6/145)

"-", designates a category that was not significantly over-represented in the given conditions up/down, number of gene transcripts either up- or down-regulated.

"EARLY RESPONDERS" TO ROSI-ACTIVATED PPARγ2

A modified GO slim analysis of the directed acyclic subgraph (see Materials and Methods Section) reveals six important categories of biological processes that are affected at 2 h, including morphogenesis, signal transduction, lipid metabolism, apoptosis, immune response, and regulation of cell differentiation (Fig. 5 and Table II). Most genes involved in cellular lipid metabolism (node 34) and negative regulation of apoptosis (node 53) were induced at 2 h and remained induced over 24 and 72 h (Fig. 5 and Table II). The expression of genes involved in the regulation of cell differentiation (node 30) was predominantly increased at all time points, however this node included adipocyte-specific, but not osteoblast-specific, genes. Interestingly, genes corresponding to the Wnt-receptor signaling pathway (node 40) show initial upregulation followed by significant downregulation at 72 h. Components of the immune system process were induced early, however myeloid cell differentiation (node 52) was upregulated at all time points, whereas T cell activation (node 35) and lymphocyte differentiation (node 51) showed diminished expression after 24 and 72 h, respectively (Fig. 5 and Table II).

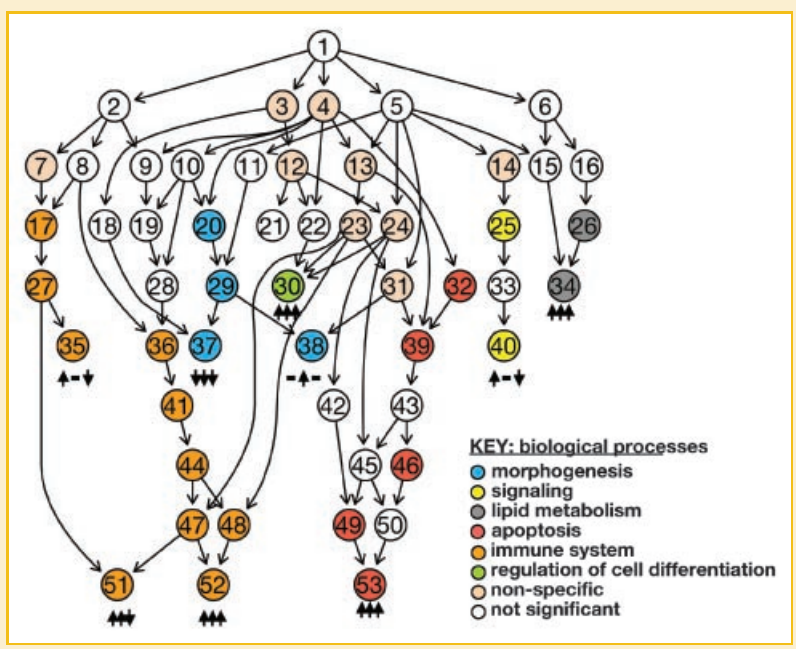

Fig. 5. "Early" responding gene transcripts to Rosi treatment in U-33/γ2 cells. Directed acyclic subgraph of biological process gene ontology terms over-represented at 2 h due to activation of U-33/γ2 cells with Rosi. The numbers are node identifiers and the colors indicate significant biological processes ($P < 0.01$). Blue, anatomical structure morphogenesis; yellow, signal transduction; light blue, lipid metabolism; red, apoptosis; orange, immune system; green, inflammatory response; beige, non-specific or general processes; and white, not significant. Arrow and dash designators underneath "leaf" nodes indicate prevailing changes for significant genes in each process at 2, 24, and 72 h, respectively. Arrows indicate up- and down-regulation while a "-" indicates that an equal number of genes in the node were up- and down-regulated at a given time point.

TABLE II. GO Term Enrichment of "Leaf" Nodes in Early Responders: (U-33/γ2 + Rosi) Versus U-33/γ2*

Cluster	Node Identifier[a]	Biological Process GO terms[b]
Morphogenesis	37	GO:0008361: regulation of cell size ($P = 7.78 \times 10^{-3}$, 5 of 115)
	38	GO:0000904: cellular morphogenesis during differentiation ($P = 8.06 \times 10^{-3}$, 6 of 163)
Signaling	40	GO:0016055: Wnt receptor signaling pathway ($P = 1.20 \times 10^{-3}$, 6 of 111)
Lipid metabolism	34	GO:0044255: cellular lipid metabolic process ($P = 5.56 \times 10^{-3}$, 12 of 483)
Apoptosis	53	GO:0043066: negative regulation of apoptosis ($P = 8.06 \times 10^{-3}$, 6 of 163)
Immune	35	GO:0042110: T cell activation ($P = 1.51 \times 10^{-3}$, 6 of 116)
	51	GO:0030098: lymphocyte differentiation ($P = 2.37 \times 10^{-3}$, 5 of 87)
	52	GO:0002573: myeloid leukocyte differentiation ($P = 1.12 \times 10^{-4}$, 5 of 45)
Cell differentiation	30	GO:0045595: regulation of cell differentiation ($P = 1.26 \times 10^{-3}$, 7 of 153)

*Gene ontology (GO) relationships are hierarchically networked sets of defined terms connected to one another in the form of a directed acyclic graph (DAG). Each GO term in the DAG is defined to be a "node." Each node in the DAG with only in-edges and no out-edges is defined to be a "leaf."
[a]Corresponding to DAG in Figure 4.
[b]Shown in parentheses is the significance of each GO term and the number of differentially expressed genes within a GO term out of the total number of genes from GO that term considered on the array.

Considerations of the expression of all 198 early responder genes exhibited three distinctive patterns of expression over time (FDR < 0.01). Table S7 provides an entire list of genes, whereas Table III lists only selected examples of genes, with either known or potential role in the regulation of adipocytic and osteoblastic phenotype.

The first group of 66 genes was characterized by consistently increased expression indicating their requirements for differentiation and the maintenance of adipocyte phenotype and function. The majority of these genes represent transcriptional regulators of adipocyte differentiation (e.g., C/EBPα and STAT5a) and genes involved in adipocyte function including adipokine production, lipid accumulation and lipid metabolism (e.g., Acox1, Adipoq, CD36, Cidec, Lipe, Lpin1, FABP4, Pnpla2, and Pex). A number of genes in this group with less characterized function: Angptl4, Aqp7, G0s2, and Ubd, achieved a very high level of expression in mature

TABLE III. "Early Responders" to Rosi Treatment (2 h) of U-33/γ2 Cells

Symbol	Gene description	FC 2	FC 24	FC 72
Category 1: Consistently up-regulated				
Acox1	Acyl-Coenzyme A oxidase 1, palmitoyl	2.3	3.8	9.5
Adfp	Adipose differentiation related protein	2.8	2.7	4.7
Adipoq	Adiponectin, C1Q and collagen domain containing	3.0	12.1	2.3
Angptl4	Angiopoietin-like 4	6.5	12.9	14.2
Aqp7	Aquaporin 7	3.8	25.9	26.0
Cd36	CD36 antigen	3.3	23.8	179.4
Cebpa	CCAAT/enhancer binding protein (C/EBP), alpha	3.1	4.1	3.4
Cidec	Cell death-inducing DFFA-like effector c	11.6	62.5	456.5
Fabp4	Fatty acid binding protein 4, adipocyte	5.7	16.9	69.8
G0s2	G0/G1 switch gene 2	4.9	43.3	35.3
Lipe	Lipase, hormone sensitive	3.2	27.8	74.7
Lpin1	Lipin 1	2.1	3.3	10.1
Pnpla2	Patatin-like phospholipase domain containing 2	2.0	21.7	60.9
Rreb1	Ras responsive element binding protein 1	2.4	2.6	2.0
Stat5a	Signal transducer and activator of transcription 5A	1.9	2.6	2.3
Tle3	Transducin-like enhancer of split 3	3.0	2.0	1.9
Tob1	Transducer of ErbB-2.1	1.8	1.8	2.2
Ubd	Ubiquitin D	1.9	3.6	41.4
Category 2: Consistently down-regulated				
BMP4	Bone morphogenic protein 4	−1.7	−8.0	−6.9
Fosl2	Fos-like antigen 2	−1.6	−1.7	−3.5
Plk2	Polo-like kinase 2	−2.6	−3.9	−5.5
Socs5	Suppressor of cytokine signaling 5	−2.0	−3.0	−3.1
Tnfsf11 (RANKL)	Tumor necrosis factor (ligand) superfamily, member 11	−1.6	−1.6	−3.7
Wisp1	WNT1 inducible signaling pathway protein 1	−2.3	−5.2	−2.6
Category 3: Temporally fluxuating				
Arhgap5	Rho GTPase activating protein 5	2.1	NS	NS
Arhgap22	Rho GTPase activating protein 22	1.3	NS	NS
Dmp1	Dentin matrix protein 1	−2.4	NS	NS
Fzd1	Frizzled homolog 1 (Drosophila)	1.7	NS	−2.0
Fzd4	Frizzled homolog 4 (Drosophila)	2.3	2.6	NS
Gprc5a	G protein-coupled receptor, family C, group 5, member A	−1.9	NS	NS
Pik3r1	Phosphatidylinositol 3-kinase, regulatory subunit (p85 alpha)	3.2	2.1	NS
Ppap2b	Phosphatidic acid phosphatase type 2B	2.5	NS	NS
Rab5b	RAB5B, member RAS oncogene family	1.8	NS	NS
Rab30	RAB30, member RAS oncogene family	−2.1	−2.0	NS
Rgs4	Regulator of G-protein signaling 4	1.5	−3.1	−1.7
Socs2	Suppressor of cytokine signaling 2	−2.5	2.4	NS

FC, fold change; NS, statistically nonsignificant change.

TABLE IV. Fold Change (FC) Expression of Representative Osteoblast-Specific Genes in (U-33/γ2 + Rosi) Versus U-33/γ2 Cells

Process	Gene symbol	Gene name	FC2	FC24	FC72	Q2	Q24	Q72	Cluster
Wnt signaling	Fzd1	Frizzled homolog 1	1.7	−1.1	−2.0	0.002	0.621	0.002	2[a]
	Fzd2	Frizzled homolog 2	−1.1	−3.3	−4.1	0.654	0.000	0.000	7
	Fzd4	Frizzled homolog 4	2.3	2.5	1.1	0.002	0.000	0.500	1[a]
	Fzd5	Frizzled homolog 5	1.2	−2.8	−6.1	0.357	0.000	0.000	7[a]
	Fzd7	Frizzled homolog 7	−1.0	1.1	−1.7	0.750	0.672	0.008	4[a]
	Frzb	Frizzled-related protein	1.1	−1.9	−2.0	0.568	0.003	0.002	7[a]
	Dkk3	Dickkopf homolog 3	−1.0	−5.0	−8.0	0.714	0.000	0.000	7[a]
	Dvl1	Dishevelled, dsh homolog 1	1.1	1.2	2.6	0.599	0.242	0.000	3
	Sfrp1	Secreted frizzled-related sequence protein 1	1.1	−2.4	−12.3	0.713	0.001	0.000	7[a]
	Wif1	Wnt inhibitory factor 1	1.5	−16.0	−72.9	0.087	0.000	0.000	7
	Wisp1	WNT1 inducible signaling pathway protein 1	−2.3	−5.2	−2.6	0.001	0.000	0.000	4
	Wisp2	WNT1 inducible signaling pathway protein 2	1.1	−1.9	−1.3	0.574	0.004	0.129	2
	Ctnnb1	Catenin beta 1	1.0	−1.5	−2.1	0.722	0.050	0.000	7
	Ctnnbip1	Catenin beta interacting protein 1	1.0	1.0	−1.6	0.734	0.751	0.026	4
	Tcf3	Transcription factor 3	−1.1	1.1	−1.8	0.705	0.643	0.009	5
	Tcf4	Transcription factor 4	1.4	−1.2	−4.4	0.157	0.413	0.000	7
	Tle3	Transducin-like enhancer of split 3	3.0	1.9	1.9	0.000	0.001	0.002	3
	Tle6	Transducin-like enhancer of split 6	−1.0	−1.5	−3.1	0.734	0.043	0.000	7
	Aes	Amino-terminal enhancer of split	1.1	−1.5	−2.6	0.611	0.105	0.000	4[a]
Tgfb/BMP/Activin signaling	Tgfb1	Transforming growth factor, beta 1	−1.2	1.8	1.5	0.392	0.003	0.037	3
	Tgfb2	Transforming growth factor, beta 2	1.4	2.0	−1.9	0.212	0.001	0.006	4
	Tgfb3	Transforming growth factor, beta 3	1.1	−1.6	−2.4	0.682	0.030	0.000	4
	Tgfbr2	Transforming growth factor, beta receptor II	−1.0	−1.5	−2.5	0.712	0.043	0.000	7[a]
	Inhbb	Inhibin beta-B	−1.1	1.6	1.8	0.605	0.023	0.003	3[a]
	Acvr1	Activin A receptor, type 1B	1.2	1.3	−1.7	0.410	0.250	0.003	5
	Fst	Follistatin	1.1	−1.9	−3.5	0.677	0.006	0.000	4
	Fstl3	Folistatin-like 3	−1.2	−1.3	−1.9	0.369	0.355	0.000	4
	Bmp4	Bone morphogenic protein 4	−1.7	−8.0	−6.9	0.027	0.000	0.000	7[a]
	Bmp2k	BMP2 inducible kinase	1.0	1.2	−2.0	0.760	0.458	0.003	4
	Bmpr2	Bone morphogenic protein receptor, type II	1.0	−1.3	−1.7	0.727	0.257	0.008	4
	Smad1	MAD homolog 1	1.1	−2.2	−5.3	0.640	0.001	0.000	4
	Smad3	MAD homolog 3	−1.5	−2.1	−2.1	0.055	0.002	0.000	7[a]
	Smad4	MAD homolog 4	−1.0	−1.7	−1.9	0.741	0.022	0.001	7[a]
	Smad7	MAD homolog 7	−1.0	−1.7	−6.2	0.738	0.037	0.000	7[a]
	Tob1	Transducer of ErbB-2.1	1.8	1.8	2.2	0.010	0.001	0.000	1
	Smurf1	SMAD specific E3 ubiquitin protein ligase 1	−1.0	1.2	1.5	0.744	0.171	0.022	3[a]
	Bambi	BMP and activin membrane-bound inhibitor	1.0	−2.9	−5.0	0.694	0.000	0.000	7
IGF signaling	Igf1	Insulin-like growth factor 1	1.9	−1.3	−2.8	0.019	0.335	0.000	5
	Igf1r	Insulin-like growth factor 1 receptor	1.1	1.1	−2.1	0.525	0.630	0.003	4
	Igf2	Insulin-like growth factor 2	−1.2	−1.1	−3.4	0.373	0.715	0.000	5
	Igfbp4	Insulin-like growth factor binding protein 4	1.3	−1.3	−2.9	0.278	0.182	0.000	5
FGF signaling	Fgfr1	Fibroblast growth factor receptor 1	−1.0	1.6	2.2	0.731	0.013	0.001	3
	Fgfr2	Fibroblast growth factor receptor 2	1.1	1.1	−3.7	0.554	0.663	0.000	5
	Fgfr3	Fibroblast growth factor receptor 3	1.1	−1.6	−7.2	0.691	0.053	0.000	5
Transcriptional regulators	Runx2	Runt related transcription factor 2	−1.4	−2.0	−7.6	0.191	0.003	0.000	7
	Dlx5	Distal-less homeobox 5	−1.6	−3.2	−7.0	0.071	0.000	0.000	7
	Sp7	Trans-acting transcription factor 7 (Osterix)	−1.1	−3.8	−5.5	0.400	0.000	0.000	7
	Twist1	Twist gene homolog 1	−1.2	−1.3	−2.1	0.469	0.227	0.000	4
	Twist2	Twist gene homolog 2	1.5	1.1	1.7	0.085	0.452	0.008	3[a]
	Sox9	SRY-box containing gene 9	−1.2	−1.2	−2.7	0.411	0.322	0.000	5[a]
Other regulators	Pthr1	Parathyroid hormone receptor 1	1.1	−1.2	−6.1	0.952	0.294	0.000	5
	Vdr	Vitamin D receptor	−1.6	−3.8	−3.9	0.012	0.000	0.000	4[a]
	Tnsfs11	Tumor necrosis factor (ligand) superfamily, member 11 (RANKL)	−1.6	−1.6	−3.7	0.004	0.049	0.000	7[a]
	Tnfrsf11b	Tumor necrosis factor receptor superfamily, member 11b (osteoprotegerin)	1.6	−2.3	1.5	0.019	0.000	0.138	4
	M-CSF1	Macrophage colony stimulating factor 1	−1.4	−5.8	−6.3	0.052	0.000	0.000	4[a]
	Il7	Interleukin 7	1.6	−1.2	−2.4	0.004	0.440	0.000	5
	Il18	Interleukin 18	1.0	−2.6	−4.3	0.739	0.000	0.000	7
	Ccnd1	Cyclin D1	−1.2	−3.8	−12.2	0.487	0.000	0.000	7[a]
	PCNA	Proliferating cell nuclear antigen	−1.2	−1.8	−2.4	0.486	0.013	0.000	4
	Mapk6	Mitogen activated protein kinase 6	−1.1	6.9	5.8	0.684	0.000	0.000	6
	Plk2	Polo-like kinase 2	−2.6	−3.9	−5.5	0.001	0.000	0.000	7[a]
	Vegfa	Vascular endothelieal growth factor A	−2.3	1.2	1.6	0.005	0.530	0.055	3
	Vegfb	Vascular endothelieal growth factor B	−1.0	1.4	2.6	0.726	0.176	0.000	1
	Vegfc	Vascular endothelieal growth factor C	1.1	−1.5	−6.9	0.608	0.114	0.000	5
	Fbxw2	F-box and WD-40 domain protein 2	−1.0	1.2	2.0	0.735	0.363	0.000	3
	Jun	Jun oncogene	−1.3	−3.0	−3.7	0.296	0.000	0.000	4
	PTN	Pleiotrophin	1.0	−4.3	−3.7	0.751	0.000	0.000	4[a]
	P2rx7	Purinergic receptor P2X, ligand-gated ion channel 7	1.2	−2.1	−3.4	0.422	0.000	0.000	4
ECM components and associated proteins	Dmp1	Dentin matrix protein 1	−2.4	−1.1	−1.0	0.006	0.674	0.739	4
	Col1a1	Procollagen type I alfa 1	−1.0	−1.8	−4.8	0.728	0.019	0.000	2[a]
	Col3a1	Procollagen type III alfa 1	1.1	−2.6	−1.3	0.634	0.000	0.358	7
	Col4a1	Procollagen type IV alfa 1	1.2	1.5	2.3	0.465	0.095	0.000	3
	Col4a5	Procollagen type IV alfa 5	1.2	−1.7	−4.7	0.416	0.023	0.000	2[a]
	Col5a1	Procollagen type V alfa 1	−1.1	−1.6	−1.2	0.660	0.028	0.416	4[a]

(*Continued*)

TABLE IV. (*Continued*)

Process	Gene symbol	Gene name	FC2	FC24	FC72	Q2	Q24	Q72	Cluster
	Col8a1	Procollagen type VIII alfa 1	−1.1	−5.3	−6.3	0.668	0.000	0.000	7[a]
	Col10a1	Procollagen type X alfa 1	1.2	1.7	1.2	0.436	0.008	0.346	1
	Col11a1	Procollagen type XI alfa 1	1.2	−11.0	−3.4	0.443	0.000	0.000	4
	Col12a1	Procollagen type XII alfa 1	1.2	−1.8	−2.3	0.414	0.019	0.000	4
	Col15a1	Procollagen type XV alfa 1	−1.0	2.0	5.4	0.741	0.002	0.000	1
	Col18a1	Procollagen type XVIII alfa 1	−1.1	−5.3	−6.3	0.668	0.000	0.000	7[a]
	Fn1	Fibronectin	1.0	−2.6	−2.1	0.716	0.000	0.001	7[a]
	Itgav	Integrin alpha V	1.0	−2.7	−3.0	0.723	0.000	0.000	4
	Itgb1	Integrin beta 1	1.0	−1.8	−2.1	0.713	0.007	0.001	4
	Ibsp	Integrin binding sialoprotein	−1.0	−9.4	−93.2	0.756	0.000	0.000	5
	Spp1	Secreted phosphoprotein 1	1.1	−1.3	−2.1	0.551	0.084	0.000	7
	Cdh11	Cadherin 11	1.3	−1.1	−3.4	0.182	0.572	0.000	5
	Bmp1	Bone morphogenic protein 1	1.0	−1.5	−1.8	0.721	0.041	0.015	4[a]
	Ctsk	Cathepsin K	1.1	−1.5	−6.4	0.666	0.083	0.000	7[a]
	Mmp2	Matrix metallopeptidase 2	−1.1	−2.3	−6.1	0.660	0.000	0.000	7
	Mmp13	Matrix metallopeptidase 13	1.1	−1.6	−2.8	0.555	0.020	0.000	5
	Phex	Phosphate regulated gene	1.4	−2.6	−19.5	0.046	0.001	0.000	5
	Akp2	Alkaline phosphatase 2	1.0	−2.5	−11.5	0.759	0.001	0.000	7
	Bgn	Biglycan	1.0	−1.1	−2.2	0.742	0.672	0.000	7
	Mgp	Matrix Gla protein	−1.7	−7.0	−4.3	0.07	0.000	0.000	2[a]
	Bglap1	Bone gamma carboxyglutamate protein 1 (osteocalcin)	1.1	−1.8	−14.9	0.600	0.001	0.000	5[a]

Q, value of false discovery rate;
[a]correlates with this cluster.

adipocytes (72 h treatment) suggesting their role in the maintenance of adipocyte phenotype. This group also includes Tle3 and Tob1, negative regulators of the pro-osteoblastic Wnt and TGFβ/BMP signaling pathways, respectively [Javed et al., 2000; Yoshida et al., 2000].

A second group of 19 genes show consistently decreased expression in response to Rosi-activated PPARγ2 in comparison with non-treated cells. This group includes known and potential positive regulators of osteoblastogenesis such as Wisp1, BMP4, Plk2, and Fosl2 (Fra-2) [Abe et al., 2000; McCauley et al., 2001; Ma et al., 2003; French et al., 2004], as well as Socs5, Ccl2 and RANKL, cytokines involved in osteoblast communication with hematopoietic environment [Boyce and Xing, 2008; O'Shea and Murray, 2008].

The third group of 113 genes is characterized by rapid upregulation or downregulation at the 2 h time point followed by a fluctuating pattern of expression. Two important regulators of phosphate homeostasis and mineralization, Phex1 and Dmp1 [Strom and Juppner, 2008], responded early to PPARγ2 with a pattern of expression over the time of treatment suggesting their involvement in the induction step of osteoblast to adipocyte conversion. For instance, after initial downregulation Dmp1 expression returned to the basal level, whereas Phex1 expression after initial upregulation was downregulated by 20-fold in differentiated adipocytes. Similarly, PPARγ2 affected expression of number of genes representing G-protein signaling family, which plays an important role in osteoblast differentiation [Hsiao et al., 2008; Peng et al., 2008; Teplyuk et al., 2008]. PPARγ2 affects early and temporally the expression of G-protein coupled receptor Gprc5a, Rho GTPase activating proteins Arhgap5 and 22, members of RAS oncogene family (Rab 5b and 30), and Rsg4 regulator.

Some of the genes, which are rapidly and temporally upregulated by Rosi may play a dual role as mediators of both, anti-osteoblastic and anti-diabetic activities of PPARγ. PIK3R1, the p85α regulatory subunit of phosphatidylinositol 3-kinase, plays an important role in insulin sensitivity and glucose homeostasis and mediation of growth factors signaling, including IGF-1 [Hallmann et al., 2003]. Socs2 negatively regulates growth hormone action and functions as a mediator of cross talk between PPARγ and growth hormone in vivo [Rieusset et al., 2004]. Animals deficient in Socs2 display an increased longitudinal skeletal growth but reduced bone mineral density, as a consequence of deregulated GH/IGF-1 signaling [Lorentzon et al., 2005]. Ppap2b, phosphatidic acid phosphatase type 2b, regulates phospholipids metabolism and might be involved in the production of PPARγ endogeneous ligands [Kanoh et al., 1999; Davies et al., 2001]. Ppap2b also interacts with Wnt pathway by inhibiting β-catenin-mediated TCF transcriptional activity [Escalante-Alcalde et al., 2003]. Thus, increased expression of Ppap2b may have two potential consequences: it may upregulate production of endogenous PPARγ ligand and/or it may contribute to downregulation of Wnt pathway pro-osteoblastic activity.

ANALYSIS OF PPRE SITES IN THE PROMOTER REGIONS OF "EARLY RESPONDERS"

Genes with increased expression after 2 h of Rosi treatment are candidates for direct regulation by PPARγ. Transcriptional activity of PPARγ involves binding to a specific regulatory sequence PPRE, which is present in upstream regions of genes regulated by this nuclear receptor. In silico analysis of 8 kb fragments located upstream of transcription start sites (TSS) for genes early regulated by Rosi-activated PPARγ2 revealed a high number of PPREs frequently organized in clusters, as compared to the occurrence of PPREs in randomly generated DNA sequences of the same length (Bonferroni-corrected *t*-test $P = 0.00004$) and upstream regions of genes characterized by Rosi-suppressed expression (*t*-test $P = 0.004$). Genes characterized by high and increasing expression over time show sixfold higher concentration of PPREs within 1 kb upstream of the TSS, as compared to random sequences and upstream regions of Rosi-suppressed genes (Fig. S4). In contrast, the frequency of PPREs in upstream regions of suppressed genes was not statistically different from the frequency recorded for random sequences (*t*-test $P = 0.1$).

PPARγ2 transcriptional control involves upregulation and downregulation of gene expression. Locating multiple PPREs clustered in the regulatory regions of upregulated genes of the adipocytic pathway suggests direct transcriptional control by PPARγ2 and a modular organization of *cis*-regulatory regions with multiple transcription factor binding sites [Heinaniemi et al., 2007]. Similarly, the lack of PPREs in the regulatory regions of downregulated genes suggests a lack of PPRE involvement. This finding is consistent with reports that PPARγ has a suppressive effect on gene expression without direct transcriptional control [Ricote and Glass, 2007].

EFFECT OF ROSI-ACTIVATED PPARγ2 ON MARKERS FOR OSTEOBLASTOGENESIS

Osteoblast differentiation and function is regulated by a network of signaling pathways, phenotype-specific transcription factors, enzymes, and structural genes that permit the formation of a collagen based extracellular matrix and its subsequent mineralization [Lian et al., 2006]. Osteoblasts also produce factors, such as macrophage colony stimulating factor (M-CSF), receptor activator of the NFκB ligand (RANKL) and its decoy receptor osteoprotegerin (OPG), which support the development of bone resorbing cells, or osteoclasts [Boyce and Xing, 2008].

Rosi-activated PPARγ2 suppresses the expression of many genes linked to signaling, transcriptional regulation of osteoblast differentiation, and extracellular matrix formation and mineralization (Table IV and Fig. 6). Early changes in gene expression are seen among members of Wnt and TGFβ/BMP signaling pathways, followed by a suppression of increasing number of pathway-specific genes with time of treatment. The pattern of gene expression specific for these pathways at the 72 h time point suggests that in cells converted to adipocytes Wnt and TGFβ/BMP pathways activities are substantially suppressed. Transcripts for essential osteoblast-specific transcription factors, such as Dlx5, Runx2, and Osterix, showed altered expression only after 24 h treatment with Rosi and continued to be downregulated in cells converted to adipocytes. This pattern of expression suggests that the anti-osteoblastic PPARγ2 effect is mediated through early responders, but not osteoblast-specific transcriptional regulators.

The effect of Rosi on osteoblast specific regulators of transcription and function is followed by changes in the expression of genes encoding large number of proteins involved in extracellular matrix formation and osteoblast function. These include different types of collagen, fibronectin, integrins, alkaline phosphatase, osteocalcin, biglycan and bone sialoprotein. The large number of genes coding for G-protein family is affected over all time points of treatment. Through their roles in cytoskeleton organization and integration of cellular signaling, this group of proteins may represent potential regulators of osteoblast-to-adipocyte conversion.

Changes in the expression of other osteoblast-specific signaling pathways, including FGF, IGF-1, and PTH, either coincide with the effect on transcriptional regulators or occur later. This pattern indicates the relative distance of these signaling pathways from direct transcriptional control by PPARγ2.

The effect of Rosi on the expression of M-CSF, RANKL, VDR, and OPG indicates that osteoblast support for osteoclastogenesis is under a direct control of PPARγ2. Even though PPARγ2 decreases the expression of pro-osteoclastic cytokines and the vitamin D receptor here, we have previously shown that this Rosi-induced anti-osteoclastic effect is completely abrogated in U-33/γ2 cells in the presence of 1,25-dihydroxyvitamin D [Lazarenko et al., 2007]. Additionally, Rosi has also been shown to induce RANKL expression in primary bone marrow cells, and Rosi administration to mice with attenuated bone formation increased bone resorption [Lazarenko et al., 2007]. Therefore, in some instances in vitro results may reflect regulatory associations between genes rather than defined transcriptional controls of their expression. In this light, our microarray

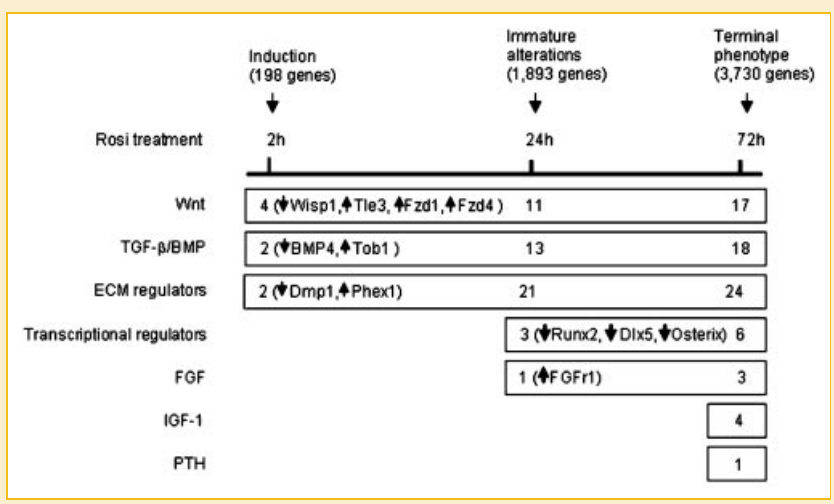

Fig. 6. Schematic representation showing the number of gene expression changes involved in osteoblast-specific signaling pathways and phenotype regulators as function of treatment duration with Rosi. Numbers in boxes represent number of pathway-specific genes with expression changes at each analyzed time point. Arrows indicate whether the expression of listed gene was up- or down-regulated at the given time point.

results indicating control of osteoclastogenesis should be interpreted in light of the biological context.

DISCUSSION

A question-driven multivariate approach was used to probe the mechanistic consequences of Rosi-activation of PPARγ2 as cells convert from an osteoblast-like to a mature adipocyte phenotype. In contrast to previous studies, which examined a static effect of Rosi-activated PPARγ2 on marrow MSC gene expression [Lecka-Czernik et al., 1999, 2002, 2007; Shockley et al., 2007], the analysis presented here describes PPARγ2-directed temporal relationships in gene expression during progression toward adipocytic and suppression of osteoblastic phenotype. The following aspects of this process were considered: (1) the sequence of events which led from osteoblastic cells to cells of the adipocytic lineage, (2) whether PPARγ2-triggered pro-adipocytic and anti-osteoblastic mechanisms share common regulatory steps, and (3) whether PPARγ2 exerts transcriptional activities in the absence of exogenous activator.

A set of early responder genes provides information about initial triggers directing cells toward the adipocyte and away from the osteoblast lineage. Our analysis indicates that the pro-adipogenic mechanism includes PPARγ2 direct transcriptional control through PPREs located in the promoter region of other transcriptional regulators and genes involved in adipocyte function. While adipocytic-induction occurred very early and continued to increase through mature fat cells, most osteoblast-related genes were downregulated after initiation of adipocyte differentiation. The exceptions include several genes, which are good candidates for initial mediators of PPARγ2 anti-osteoblastic activity. These candidates consist of two transcripts encoding negative regulators of osteoblastogenesis (Tle3 and Tob1), and several transcripts which encode for known or potential positive regulators of osteoblastogenesis (e.g., Wisp1, BMP4, and Dmp1, Phex1). Interestingly, these genes function in the regulation of extracellular signaling. Thus, in contrast to the pro-adipocytic mechanism which involves direct effect on transcriptional regulators, the anti-osteoblastic mechanism is triggered by an effect on signaling pathways which, in turn, downregulates the expression osteoblast-specific transcriptional regulators. Without ruling out cross-talk between processes, we postulate that different mechanisms drive PPARγ2-mediated pro-adipocytic and anti-osteoblastic effects. This proposition is consistent with previous evidence that osteoblastic repression and adipocytic induction can be distinguished and are independently regulated [Lecka-Czernik and Suva, 2006].

The late effect of PPARγ2 on the activity of other pathways, such as FGF, IGF-1, and PTH, indicates their relative distance from the PPARγ2 direct control and suggests that their suppression results from either PPARγ2 negative effect on other signalings or osteoblast-specific transcriptional regulators. This pattern implies a hierarchical structure of PPARγ2-initiated negative regulation of osteoblast differentiation and suggests that PPARγ2 anti-osteoblastic activity involves pleiotropic interactions between signaling processes and transcriptional regulators over time.

Differences between U-33/γ2 and U-33/c cell types underscore the activity of PPARγ2 even without an activating ligand. Our results demonstrate that PPARγ2 alone modulates mesenchymal stem cell phenotype in a cell culture model. It suppresses the cell cycle response and affects the expression of genes specific for the maintenance of stem cell phenotype. We have previously showed that PPARγ2 suppresses the expression of "stemness" genes including Lif and Lif receptor, while increasing the expression of genes supporting hematopoiesis including Kitl, RANKL, and the ligands for CXC chemokines [Shockley et al., 2007]. In light of increased PPARγ2 expression in aged marrow MSCs, these findings suggest that PPARγ2 may be a factor responsible for age-related changes in MSCs differentiation potential toward adipocytes and osteoblasts [Moerman et al., 2004].

In conclusion, our study shows that PPARγ2 is a major regulator of bone marrow MSC differentiation and provides information about hierarchical interactions between different regulatory pathways involved in fat- and bone-cell development. Marrow-derived adipocytes produce an expression signature that is similar to known adipocytic cells with respect to fatty acid metabolism, carbohydrate metabolism, and adipokine production. Most importantly, we provide a database of triggers and temporal expression patterns that should be helpful in our search to identify regulatory mechanisms by which PPARγ2 controls osteoblast differentiation.

ACKNOWLEDGMENTS

This study was supported by grant NIH/NIA/NIAMS (AG17482 and AG028935 to B.L.C.), American Diabetes Association (1-03-RA-46 to B.L.C.), and NIH/NHGRI Ruth L. Kirchstein Postdoctoral Fellowship (HG003968 to K.R.S.).

REFERENCES

Abe E, Yamamoto M, Taguchi Y, Lecka-Czernik B, O'Brian CA, Economides AN, Stahl N, Jilka RL, Manolagas SC. 2000. Essential requirement of BMPs-2/4 for both osteoblast and osteoclast formation in murine bone marrow cultures from adult mice: Antagonism by noggin. J Bone Miner Res 15:663–673.

Ackert-Bicknell CL, Demissie S, de Evsikova CM, Hsu YH, Demambro VE, Karasik D, Cupples LA, Ordovas JM, Tucker KL, Cho K, Canalis E, Paigen B, Churchill GA, Forejt J, Beamer WG, Ferrari S, Bouxsein ML, Kiel DP, Rosen CJ. 2008. A PPARG by dietary fat interaction influences bone mass in mice and humans. J Bone Miner Res 9:1398–1408.

Akune T, Ohba S, Kamekura S, Yamaguchi M, Chung UI, Kubota N, Terauchi Y, Harada Y, Azuma Y, Nakamura K, Kadowaki T, Kawaguchi H. 2004. PPARgamma insufficiency enhances osteogenesis through osteoblast formation from bone marrow progenitors. J Clin Invest 113:846–855.

Ali AA, Weinstein RS, Stewart SA, Parfitt AM, Manolagas SC, Jilka RL. 2005. Rosiglitazone causes bone loss in mice by suppressing osteoblast differentiation and bone formation. Endocrinology 146:1226–1235.

Ashburner M, Ball CA, Blake JA, Botstein D, Butler H, Cherry JM, Davis AP, Dolinski K, Dwight SS, Eppig JT, Harris MA, Hill DP, Issel-Tarver L, Kasarskis A, Lewis S, Matese JC, Richardson JE, Ringwald M, Rubin GM, Sherlock G. 2000. Gene ontology: Tool for the unification of biology. The Gene Ontology Consortium. Nat Genet 25:25–29.

Boyce BF, Xing L. 2008. Functions of RANKL/RANK/OPG in bone modeling and remodeling. Arch Biochem Biophys 473:139–146.

Churchill GA. 2004. Using ANOVA to analyze microarray data. Biotechniques 37:173–175. 177.

Cock TA, Back J, Elefteriou F, Karsenty G, Kastner P, Chan S, Auwerx J. 2004. Enhanced bone formation in lipodystrophic PPARgamma(hyp/hyp) mice relocates haematopoiesis to the spleen. EMBO Rep 5:1007–1012.

Cui X, Hwang JT, Qiu J, Blades NJ, Churchill GA. 2005. Improved statistical tests for differential gene expression by shrinking variance components estimates. Biostatistics 6:59–75.

Davies SS, Pontsler AV, Marathe GK, Harrison KA, Murphy RC, Hinshaw JC, Prestwich GD, St Hilaire A, Prescott SM, Zimmerman GA, McIntyre TM. 2001. Oxidized phospholipids are specific, high affinity PPAR{gamma} ligands and agonists. J Biol Chem 26:26.

Escalante-Alcalde D, Hernandez L, Le Stunff H, Maeda R, Lee HS Jr, Gang C, Sciorra VA, Daar I, Spiegel S, Morris AJ, Stewart CL. 2003. The lipid phosphatase LPP3 regulates extra-embryonic vasculogenesis and axis patterning. Development 130:4623–4637.

Falcon S, Gentleman R. 2007. Using GOstats to test gene lists for GO term association. Bioinformatics 23:257–258.

French DM, Kaul RJ, D'Souza AL, Crowley CW, Bao M, Frantz GD, Filvaroff EH, Desnoyers L. 2004. WISP-1 is an osteoblastic regulator expressed during skeletal development and fracture repair. Am J Pathol 165:855–867.

Gautier L, Cope L, Bolstad BM, Irizarry RA. 2004. affy—Analysis of Affymetrix GeneChip data at the probe level. Bioinformatics 20:307–315.

Gimble JM, Zvonic S, Floyd ZE, Kassem M, Nuttall ME. 2006. Playing with bone and fat. J Cell Biochem 98:251–266.

Grey A, Bolland M, Gamble G, Wattie D, Horne A, Davidson J, Reid IR. 2007. The peroxisome-proliferator-activated receptor-gamma agonist rosiglitazone decreases bone formation and bone mineral density in healthy postmenopausal women: A randomized, controlled trial. J Clin Endocrinol Metab 92:1305–1310.

Hallmann D, Trumper K, Trusheim H, Ueki K, Kahn CR, Cantley LC, Fruman DA, Horsch D. 2003. Altered signaling and cell cycle regulation in embryonal stem cells with a disruption of the gene for phosphoinositide 3-kinase regulatory subunit p85alpha. J Biol Chem 278:5099–5108.

Heinaniemi M, Uski JO, Degenhardt T, Carlberg C. 2007. Meta-analysis of primary target genes of peroxisome proliferator-activated receptors. Genome Biol 8:R147.

Hsiao EC, Boudignon BM, Chang WC, Bencsik M, Peng J, Nguyen TD, Manalac C, Halloran BP, Conklin BR, Nissenson RA. 2008. Osteoblast expression of an engineered Gs-coupled receptor dramatically increases bone mass. Proc Natl Acad Sci USA 105:1209–1214.

Ihaka R, Gentleman R. 1996. R: A language for data analysis and graphics. J Comput Graphical Statistics 5:299–314.

Irizarry RA, Bolstad BM, Collin F, Cope LM, Hobbs B, Speed TP. 2003. Summaries of Affymetrix GeneChip probe level data. Nucleic Acids Res 31:e15.

Javed A, Guo B, Hiebert S, Choi JY, Green J, Zhao SC, Osborne MA, Stifani S, Stein JL, Lian JB, van Wijnen AJ, Stein GS. 2000. Groucho/TLE/R-esp proteins associate with the nuclear matrix and repress RUNX (CBF(alpha)/AML/PEBP2(alpha)) dependent activation of tissue-specific gene transcription. J Cell Sci 113(Pt 12): 2221–2231.

Kahn SE, Haffner SM, Heise MA, Herman WH, Holman RR, Jones NP, Kravitz BG, Lachin JM, O'Neill MC, Zinman B, Viberti G. 2006. Glycemic durability of rosiglitazone, metformin, or glyburide monotherapy. N Engl J Med 355:2427–2443.

Kahn SE, Zinman B, Lachin JM, Haffner SM, Herman WH, Holman RR, Kravitz BG, Yu D, Heise MA, Aftring RP, Viberti G. 2008. Rosiglitazone-associated fractures in type 2 diabetes: An analysis from a diabetes outcome progression trial (ADOPT). Diabetes Care 31:845–851.

Kanoh H, Kai M, Wada I. 1999. Molecular characterization of the type 2 phosphatidic acid phosphatase. Chem Phys Lipids 98:119–126.

Kerr MK, Churchill GA. 2001. Bootstrapping cluster analysis: Assessing the reliability of conclusions from microarray experiments. Proc Natl Acad Sci USA 98:8961–8965.

Kerr MK, Martin M, Churchill GA. 2000. Analysis of variance for gene expression microarray data. J Comput Biol 7:819–837.

Lazarenko OP, Rzonca SO, Suva LJ, Lecka-Czernik B. 2006. Netoglitazone is a PPAR-gamma ligand with selective effects on bone and fat. Bone 38:74–85.

Lazarenko OP, Rzonca SO, Hogue WR, Swain FL, Suva LJ, Lecka-Czernik B. 2007. Rosiglitazone induces decreases in bone mass and strength that are reminiscent of aged bone. Endocrinology 148:2669–2680.

Lecka-Czernik B, Suva LJ. 2006. Resolving the two ''Bony'' faces of PPAR-gamma. PPAR Res 2006:27489.

Lecka-Czernik B, Gubrij I, Moerman EA, Kajkenova O, Lipschitz DA, Manolagas SC, Jilka RL. 1999. Inhibition of Osf2/Cbfa1 expression and terminal osteoblast differentiation by PPAR-gamma 2. J Cell Biochem 74:357–371.

Lecka-Czernik B, Moerman EJ, Grant DF, Lehmann JM, Manolagas SC, Jilka RL. 2002. Divergent effects of selective peroxisome proliferator-activated receptor-gamma 2 ligands on adipocyte versus osteoblast differentiation. Endocrinology 143:2376–2384.

Lecka-Czernik B, Ackert-Bicknell C, Adamo ML, Marmolejos V, Churchill GA, Shockley KR, Reid IR, Grey A, Rosen CJ. 2007. Activation of peroxisome proliferator-activated receptor gamma (PPARgamma) by rosiglitazone suppresses components of the insulin-like growth factor regulatory system in vitro and in vivo. Endocrinology 148:903–911.

Lehrke M, Lazar MA. 2005. The many faces of PPARgamma. Cell 123:993–999.

Lian JB, Stein GS, Javed A, van Wijnen AJ, Stein JL, Montecino M, Hassan MQ, Gaur T, Lengner CJ, Young DW. 2006. Networks and hubs for the transcriptional control of osteoblastogenesis. Rev Endocr Metab Disord 7:1–16.

Lorentzon M, Greenhalgh CJ, Mohan S, Alexander WS, Ohlsson C. 2005. Reduced bone mineral density in SOCS-2-deficient mice. Pediatr Res 57:223–226.

Ma S, Charron J, Erikson RL. 2003. Role of Plk2 (Snk) in mouse development and cell proliferation. Mol Cell Biol 23:6936–6943.

McCauley LK, Koh-Paige AJ, Chen H, Chen C, Ontiveros C, Irwin R, McCabe LR. 2001. Parathyroid hormone stimulates fra-2 expression in osteoblastic cells in vitro and in vivo. Endocrinology 142:1975–1981.

Moerman EJ, Teng K, Lipschitz DA, Lecka-Czernik B. 2004. Aging activates adipogenic and suppresses osteogenic programs in mesenchymal marrow stroma/stem cells: The role of PPAR-gamma2 transcription factor and TGF-beta/BMP signaling pathways. Aging Cell 3:379–389.

O'Shea JJ, Murray PJ. 2008. Cytokine signaling modules in inflammatory responses. Immunity 28:477–487.

Peng J, Bencsik M, Louie A, Lu W, Millard S, Nguyen P, Burghardt A, Majumdar S, Wronski TJ, Halloran B, Conklin BR, Nissenson RA. 2008. Conditional expression of a Gi-coupled receptor in osteoblasts results in trabecular osteopenia. Endocrinology 149:1329–1337.

Rhee EJ, Oh KW, Lee WY, Kim SY, Oh ES, Baek KH, Kang MI, Kim SW. 2005. The effects of C161→T polymorphisms in exon 6 of peroxisome proliferator-activated receptor-gamma gene on bone mineral metabolism and serum osteoprotegerin levels in healthy middle-aged women. Am J Obstet Gynecol 192:1087–1093.

Ricote M, Glass CK. 2007. PPARs and molecular mechanisms of transrepression. Biochim Biophys Acta 1771:926–935.

Rieusset J, Seydoux J, Anghel SI, Escher P, Michalik L, Soon Tan N, Metzger D, Chambon P, Wahli W, Desvergne B. 2004. Altered growth in male peroxisome proliferator-activated receptor gamma (PPARgamma) heterozygous mice: Involvement of PPARgamma in a negative feedback regulation of growth hormone action. Mol Endocrinol 18:2363–2377.

Rosen ED, Spiegelman BM. 2001. PPARgamma: A nuclear regulator of metabolism, differentiation, and cell growth. J Biol Chem 276:37731–37734.

Rzonca SO, Suva LJ, Gaddy D, Montague DC, Lecka-Czernik B. 2004. Bone is a target for the antidiabetic compound rosiglitazone. Endocrinology 145:401–406.

Saldanha AJ. 2004. Java Treeview—Extensible visualization of microarray data. Bioinformatics 20:3246–3248.

Schwartz AV, Sellmeyer DE, Vittinghoff E, Palermo L, Lecka-Czernik B, Feingold KR, Strotmeyer ES, Resnick HE, Carbone L, Beamer BA, Won Park S, Lane NE, Harris TB, Cummings SR. 2006. Thiazolidinedione (TZD) use and bone loss in older diabetic adults. J Clin Endocrinol Metab 91:3349–3354.

Sharma AM, Staels B. 2007. Review: Peroxisome proliferator-activated receptor gamma and adipose tissue—Understanding obesity-related changes in regulation of lipid and glucose metabolism. J Clin Endocrinol Metab 92:386–395.

Shockley KR, Rosen CJ, Churchill GA, Lecka-Czernik B. 2007. PPARγ2 regulates a molecular signature of marrow mesenchymal stem cells. PPAR Res 2007:81219.

Soroceanu MA, Miao D, Bai XY, Su H, Goltzman D, Karaplis AC. 2004. Rosiglitazone impacts negatively on bone by promoting osteoblast/osteocyte apoptosis. J Endocrinol 183:203–216.

Sosinsky A, Bonin CP, Mann RS, Honig B. 2003. Target Explorer: An automated tool for the identification of new target genes for a specified set of transcription factors. Nucleic Acids Res 31:3589–3592.

Sottile V, Seuwen K, Kneissel M. 2004. Enhanced marrow adipogenesis and bone resorption in estrogen-deprived rats treated with the PPARgamma agonist BRL49653 (rosiglitazone). Calcif Tissue Int 75:329–337.

Storey JD. 2002. A direct approach to false discovery rates. J Roy Statist Soc B 64:479–498.

Strom TM, Juppner H. 2008. PHEX, FGF23, DMP1 and beyond. Curr Opin Nephrol Hypertens 17:357–362.

Teplyuk NM, Galindo M, Teplyuk VI, Pratap J, Young DW, Lapointe D, Javed A, Stein JL, Lian JB, Stein GS, van Wijnen AJ. 2008. Runx2 regulates G-protein coupled signaling pathways to control growth of osteoblast progenitors. J Biol Chem 283:27585–27597.

Villesen P. 2007. FaBox: An online toolbox for FASTA sequences. Mol Ecol Notes 7:965–968.

Wan Y, Chong LW, Evans RM. 2007. PPAR-gamma regulates osteoclastogenesis in mice. Nat Med 13:1496–1503.

Yang H, Churchill G. 2007. Estimating p-values in small microarray experiments. Bioinformatics 23:38–43.

Yoshida Y, Tanaka S, Umemori H, Minowa O, Usui M, Ikematsu N, Hosoda E, Imamura T, Kuno J, Yamashita T, Miyazono K, Noda M, Noda T, Yamamoto T. 2000. Negative regulation of BMP/Smad signaling by Tob in osteoblasts. Cell 103:1085–1097.

Zandbergen F, Mandard S, Escher P, Tan NS, Patsouris D, Jatkoe T, Rojas-Caro S, Madore S, Wahli W, Tafuri S, Muller M, Kersten S. 2005. The G0/G1 switch gene 2 is a novel PPAR target gene. Biochem J 392:313–324.